ИНСТИТУТ ЯДЕРНОЙ ФИЗИКИ СО АН СССР

B.V. Chirikov and V.V. Vecheslavov

CHAOTIC DYNAMICS OF COMET HALLEY

PREPRINT 86-184

НОВОСИБИРСК

Chaotic Dynamics of Comet Halley

B.V. Chirikov and V.V. Vecheslavov

Institute of Nuclear Physics
630090, Novosibirsk, USSR

ABSTRACT

A simple model of the dynamics of Halley's comet is developed, and its motion is shown to be chaotic. Estimates for the error growth in the extrapolation of comet's trajectory are obtained. Various mechanisms limiting the full sojourn time of the comet in the solar system are considered. This time is found to crucially depend on weak nongravitational forces.

1. INTRODUCTION

Celestial mechanics, i. e. the dynamics of the solar system, has been always a perfect example of the regular, deterministic, motion which allows a long-term prediction to a fairly high accuracy. Yet, as in almost any other many-dimensional nonlinear oscillator system, the motion of a qualitatively different nature is possible here. We mean the so called dynamical chaos when a trajectory becomes random, i. e. highly irregular and unpredictable, irrespective of any noise (see, e. g., Refs [1, 2], and [3]). Moreover, according to Arnold's conjecture [4] which has been well confirmed in numerical experiments [1, 5], the chaotic components of motion for the special initial conditions of a positive measure is a generic phenomenon in nonlinear oscillations. The origin of chaos lies in a neighborhood of any separatrix, the trajectory with zero frequency of the unperturbed motion.

In celestial mechanics the simplest example of separatrix is the parabolic trajectory in the two-body problem which separates the bounded and unbounded motions. As is well known by now [1, 2, 5], in this case any perturbation, particularly, a regular one, by a uniformly rotating third body, for instance, produces a finite chaotic layer at the side of unperturbed elliptic trajectories. It has been explicitly shown in recent paper [6] for a particular case of the plane circular restricted three-body problem.

The orbits close to parabolic, i. e. ones of a large eccentricity $\varepsilon \to 1$ $(0 < 1-\varepsilon \ll 1)$, are typical for comets, those «probe particles»

in celestial mechanics. The most detailed observational data have been cumulated on the famous comet Halley which left the tracks in various historical records back to year −239 (240 B.C.). The analysis of these data allowed us to conclude that the motion of Halley's comet is chaotic. We present some of its statistical characteristics, particularly, the diffusion rate in energy, the estimates for comet's life time in the solar system, and the increment of its motion local instability which sets the limit for the extrapolation of comet's trajectory in both directions of time.

Our analysis is based upon the construction of a simple 2-dim. model (a map) for the comet dynamics, and on the subsequent study of this model by means of the modern theory of dynamical systems.

The motion of comet Halley seems to be the first real example of dynamical chaos in celestial mechanics. Another one is likely to be Saturn's satellite Hyperion as predicted by Wisdom and coworkers (see Ref. [3]). Extensive numerical simulations of the dynamics of Halley's comet [7—12] is a striking illustration of the difficulties and limitations in prediction of a chaotic motion.

2. THE MODEL

The strong instability of a chaotic trajectory restricts its extrapolation by a relatively short time interval irrespective of the modelling accuracy. On the other hand, for studying statistical properties of the motion one can use a relatively simple model which includes the essential part of dynamics of the real system. In the problem under consideration it is the dynamics of the phase of comet perturbation by Jupiter. As a conjugate variable it is convenient to choose some quantity proportional to comet's energy which determines the motion period and, hence, a change in the perturbation phase.

In constructing the model we have used, as the original data, 46 values of t_n, the comet perihelion passage time, as presented in Ref. [7] and repeated in Table 1 (t_1 value is from Ref. [8]). Values t_n comprise a fairly big time span from 1986 back to −1403 yr. Notice that only 27 values ($n=2-28$) are reconciled with the observations while the remaining 18 ones ($n=29-46$) have been predicted from the numerical simulation of comet's orbit [7].

Define the global perturbation phase via Jupiter's position, with

respect to comet's orbit, at a perihelion passage time:

$$X_n=\frac{t_n}{P_J} \tag{1}$$

and set $X_1=0$ (Table 1). Jupiter is assumed to move uniformly in a circular orbit with an effective period $P_J=4332.653$ days. As a matter of fact, P_J includes various perturbations, particularly, Jupiter's and comet's orbit precession. The above P_J value has been empirically adjusted from the best intrinsic agreement of the original data t_n (see below). Measured in years P_J is close to the ratio of Earth's and Jupiter's mean motions.

Comet's period is $P_n=t_n-t_{n-1}$. Define a quantity

$$w_n=\left(\frac{P_n}{P_J}\right)^{-2/3}=(X_n-X_{n-1})^{-2/3}\approx -2E_n, \tag{2}$$

where E_n is comet's total energy, far from Jupiter within the interval (t_{n-1}, t_n). We set Jupiter's velocity and radius of the orbit to be unity while its mass $\mu_J=9.54\times10^{-4}$ is the small perturbation parameter. The time unit is then $P_J/2\pi=689.563$ days $=1.888$ years.

The change in w depends on the perturbation phase $x=X \bmod 1$. Together with Eq. (2) it leads to a canonical map of the plane (w, x) (cf. Ref. [6]):

$$w_{n+1}=w_n+F(x_n); \quad x_{n+1}=x_n+w_{n+1}^{-3/2}. \tag{3}$$

Apparently, it is the simplest (very restricted though) model of comet's dynamics (backwards in time).

The unknown perturbation function $F(x)$ can be found directly from the original data t_n (Table 1) using the same Eqs (3). The result is depicted in Fig. 1. The scattering of points turned out to be caused by Saturn's perturbation.

The two perturbations can be separated off as follows. Approximate the dependence in Fig. 1 by a Fourier series $F_J(x)$ and plot the difference $F(x_n)-F_J(x_n)$ vs. Saturn's phase $y=Y \bmod 1$ where $Y=r_S X$ (Table 1), and $r_S=0.4026868$ is Saturn's revolution frequency. The latter has been also empirically adjusted and turned out to be equal to the ratio of Saturn's and Jupiter's mean motions. The difference $F-F_J$ as a function of y was again approximated by another Fourier series $F_S(y)$, and the whole procedure repeated for the function $F(x_n)-F_S(y_n)$ instead of the initial $F(x_n)$. After about 10 such successive approximations the following decomposition of

Table 1

Comet Halley's Dynamics: Perihelion Passage Times [7]

n	Year	Perihelion passage, t_n (JD)	Jupiter's phase X_n	Saturn's phase Y_n
1	1986	2446470.9518*	0.	0.
2	1910	2418781.6777	6.39083584	2.57350511
3	1835	2391598.9387	12.6647606	5.09993167
4	1759	2363592.5608	19.1287858	7.70290915
5	1682	2335655.7807	25.5767473	10.2994180
6	1607	2308304.0406	31.8896785	12.8415519
7	1531	2280492.7385	38.3086791	15.4263986
8	1456	2253022.1326	44.6490451	17.9795802
9	1378	2224686.1872	51.1891362	20.6131884
10	1301	2196546.0819	57.6840264	23.2285948
11	1222	2167664.3229	64.3500942	25.9129322
12	1145	2139377.0609	70.8789490	28.5420157
13	1066	2110493.4340	77.5454480	31.2265267
14	989	2082538.1876	83.9976717	33.8247519
15	912	2054365.1743	90.5001572	36.4432169
16	837	2026830.7700	96.8552482	39.0023280
17	760	1998788.1713	103.327633	41.6086720
18	684	1971164.2668	109.703382	44.1761014
19	607	1942837.9758	116.241244	46.8088124
20	530	1914909.6300	122.687259	49.4045374
21	451	1885963.7491	129.368127	52.0948344
22	374	1857707.8424	135.889745	54.7210039
23	295	1828915.8984	142.535083	57.3969935
24	218	1800819.2235	149.019949	60.0083634
25	141	1772638.9340	155.524114	62.6275046
26	66	1745189.4601	161.859602	65.1787221
27	−11	1717323.3485	168.291253	67.7686629
28	−86	1689863.9617	174.629030	70.3208017
29	−163	1661838.0660	181.097560	72.9255932
30	−239	1633907.6180	187.544060	75.5215136
31	−314	1606620.0237	193.842186	78.0576857
32	−390	1578866.8690	200.247766	80.6371280
33	−465	1551414.7388	206.583867	83.1885924
34	−539	1524318.3270	212.837867	85.7069955
35	−615	1496638.0035	219.226637	88.2796687
36	−689	1469421.7792	225.508291	90.8092075
37	−762	1442954.0301	231.617192	93.2691812

Table 1 (continued)

n	Year	Perihelion passage, t_n (JD)	Jupiter's phase X_n	Saturn's phase Y_n
38	−835	1416202.8066	237.791521	95.7555018
39	−910	1388819.7203	244.111687	98.3005491
40	−985	1361622.0640	250.389054	100.828362
41	−1058	1334960.1638	256.542767	103.306381
42	−1128	1309149.3447	262.500045	105.705298
43	−1197	1283983.7325	268.308406	108.044248
44	−1265	1259263.8959	274.013879	110.341767
45	−1333	1234416.0059	279.748908	112.651187
46	−1403	1208900.1811	285.638100	115.022687

* after [8].
Effective periods for Jupiter 4332.653; for Saturn 10759.362 (days).

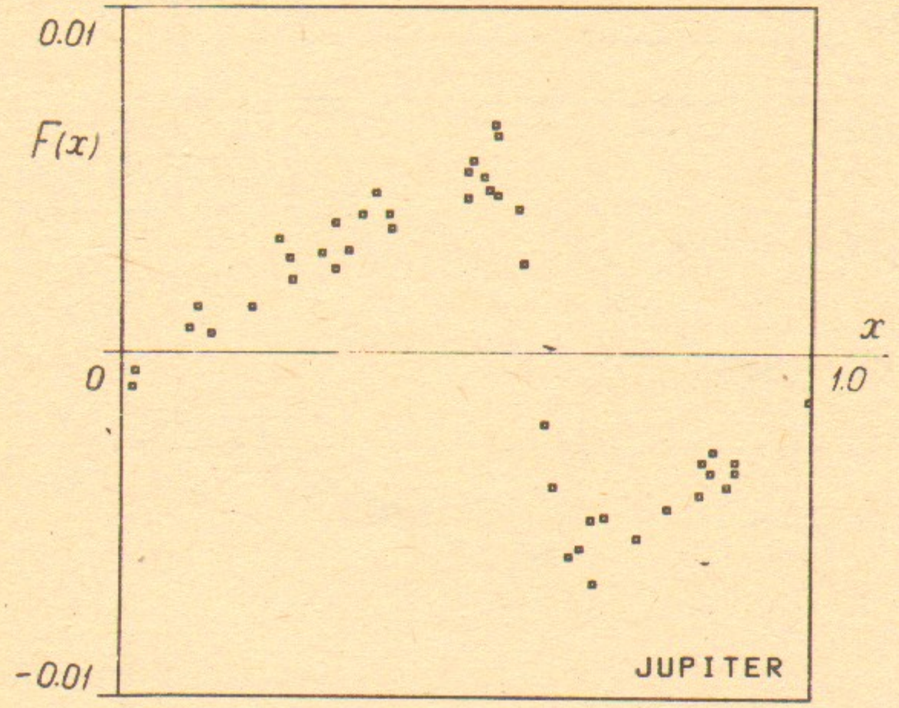

Fig. 1. The full perturbation of comet Halley vs. Jupiter's phase.

a

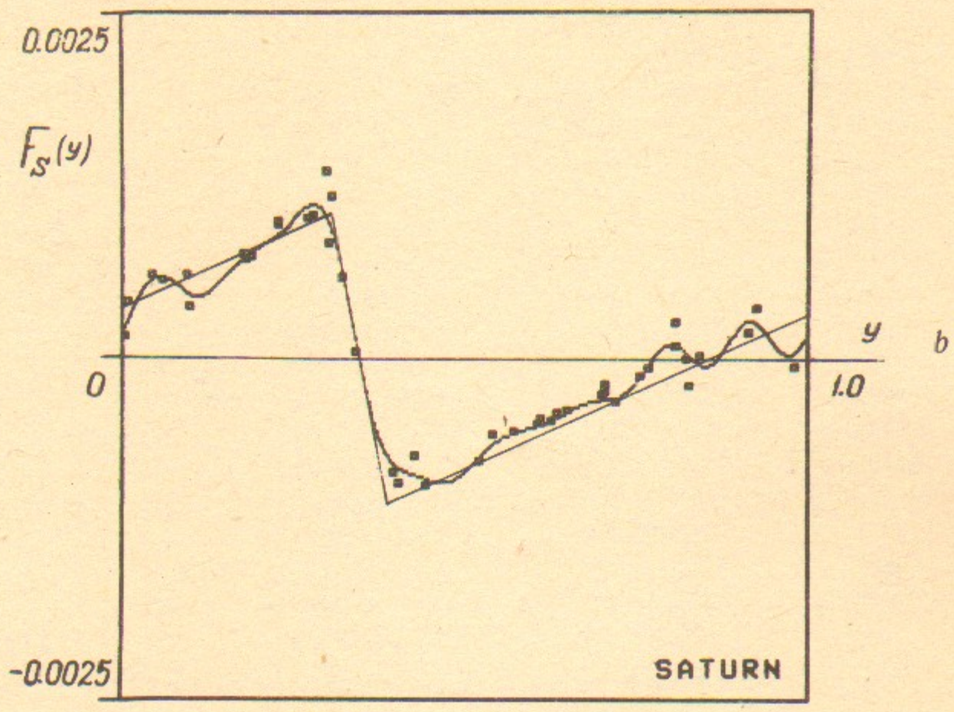

b

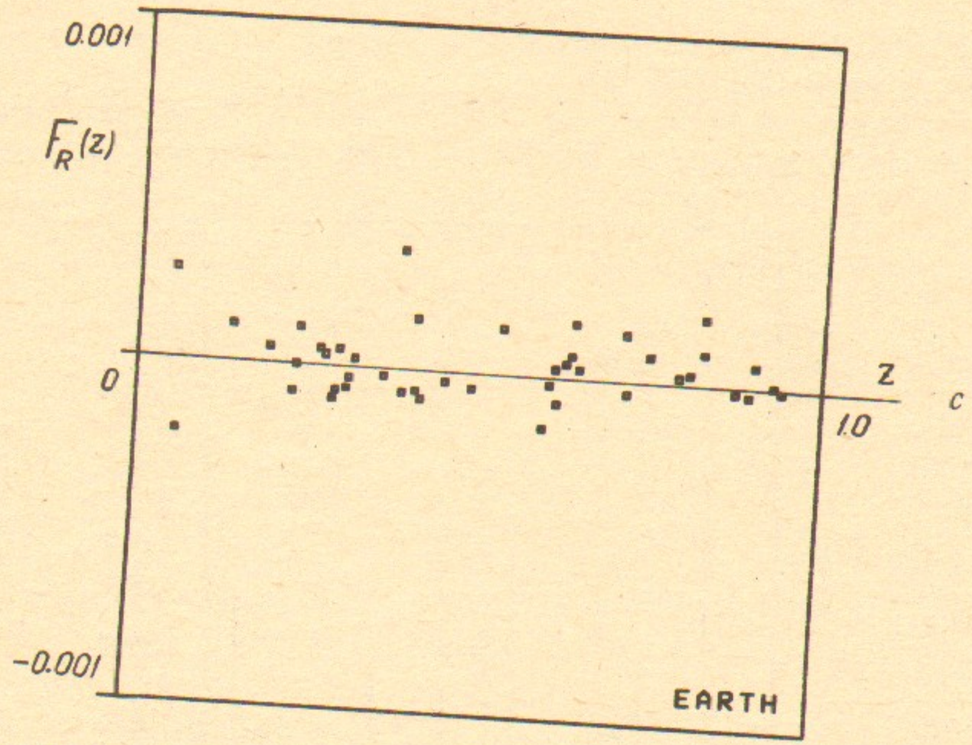

c

Fig. 2. Comet Halley's perturbation by Jupiter (*a*), by Saturn (*b*), and residual perturbation (*c*). Curves are Fourier approximation (FA), straight lines are «saw-tooth» approximation (STA).

the total perturbation into that by Jupiter, and by Saturn has been obtained (Fig. 2):

$$F(x) = F_J(x) + F_S(y) + F_R(z)\,. \tag{4}$$

The final perturbation Fourier spectrum is shown in Table 2 where

$$F_J(x) = \sum_m [a_m \cos(2\pi mx) + b_m \sin(2\pi mx)]$$

for Jupiter, and similarly for Saturn. In Fig. 2,*c* the residual perturbation $F_R(z)$ is also plotted vs. Earth's phase $z = Z \bmod 1$ where $Z = r_E X$, and $r_E = P_J$ (years) $= 11.86241$ is Earth's frequency in the units assumed. We failed to find any simple dynamical interpretation for F_R which, thus, characterizes the accuracy of our model (3):

$$\left(\frac{\langle F_R^2\rangle}{\langle F_J^2\rangle}\right)^{1/2}\approx 0.030;\quad \frac{\langle F_R^2\rangle^{1/2}}{w}\approx 3.5\times 10^{-4};\quad \langle(\Delta t)^2\rangle^{1/2}\approx 14\ \text{days}. \tag{5}$$

Here Δt is the error in «prediction» of the next (or preceding) perihelion passage time (Fig. 3).

In the process of successive approximating F_J, F_S the parameters P_J and r_S, as well as the number of Fourier harmonics, have been

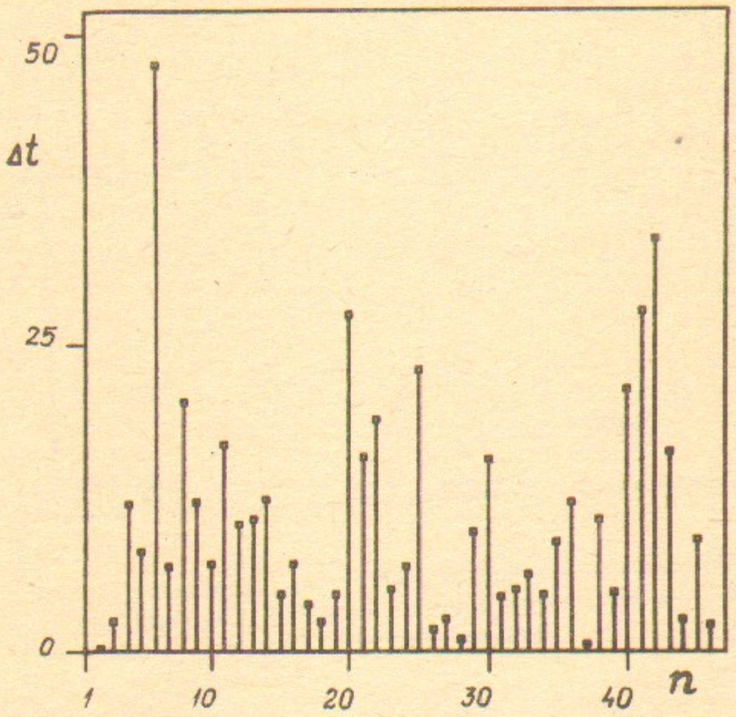

Fig. 3. Accuracy of model (3) for comet Halley's dynamics: Δt (days) is the prediction error of perihelion passage time t_n from the two preceding values t_{n-1} and t_{n-2}.

also optimized by minimizing residual $\langle F_R^2\rangle$. Interestingly, the optimizing proved to be very sensitive to P_J value, so that the empirical uncertainty in this model parameter is only 0.01 day$\approx$15 min! Similarly, the relative uncertainty of effective Saturn's frequency r_S is $\sim 10^{-6}$.

The developed model (3), together with the empirical perturbation (Table 2) is, of course, but a physically meaningful interpolation of the original data t_n.

Besides the Fourier approximation (FA) of perturbation we made also use of a simpler «saw-tooth» approximation (STA)

Table 2

Perturbation Fourier Spectrum in Model (3)

m	Jupiter			Saturn		
	$a_m\times 10^2$	$b_m\times 10^2$	$\sqrt{a_m^2+b_m^2}\times 10^2$	$a_m\times 10^3$	$b_m\times 10^3$	$\sqrt{a_m^2+b_m^2}\times 10^3$
0	0	0	0	0	0	0
1	−.240980	.390305	.458704	.539282	.402058	.672663
2	.182350	−.060684	.192182	−.365971	.094560	.377990
3	−.120144	−.025157	.122749	.055456	−.195876	.203575
4	.053170	.062750	.082247	.087232	.145022	.169236
5	−.002350	−.051279	.051333	−.076651	.043299	.088035
6	−.019543	.033955	.039178	−.019011	−.032018	.037237
7	.019810	−.006757	.020931	−.010290	.049478	.050537
8	−.016521	−.005454	.017398	−.067932	.063112	.092724
9	.003908	.009710	.010467	−.000503	.012022	.012033
10	−.001400	−.005662	.005833	.013116	.013741	.018996

when each of the functions $F_J(x)$, $F_S(y)$ was represented by the two straight lines as shown in Fig. 2. The amplitudes and vertex positions have been assumed as follows

$$\begin{aligned} &A_J=6.35\times 10^{-3};\quad x_+=0.552;\quad x_-=0.640;\\ &A_S=1.05\times 10^{-3};\quad y_+=0.305;\quad y_-=0.385;\\ &2d_J=x_--x_+=0.088;\quad 2d_S=y_--y_+=0.080. \end{aligned} \tag{6}$$

Naturally, the accuracy of the latter approximation is much worse (cf. Eq. (5)):

$$\left(\frac{\langle F_R^2\rangle}{\langle F_J^2\rangle}\right)^{1/2}\approx 0.10;\quad \frac{\langle F_R^2\rangle^{1/2}}{w}\approx 1.2\times 10^{-3};\quad \langle(\Delta t)^2\rangle^{1/2}\approx 50\ \text{days}.$$

We mention that the dynamics of 2-dim. maps with a «saw-tooth» perturbation, similar to map (3), was studied in Refs [13, 14] (see also Refs [1, 5]).

A surprisingly sharp phase dependence of the perturbation (Fig. 2) is explained by relatively close encounters of the comet and planets due to a small inclination angle i of comet's orbit

($\sin i \approx 0.3$). Indeed, two encounters per turn are possible, both proving to correspond approximately to the same phases x and y. Recall that we define the perturbation phase at the perihelion passage time while the perturbation actually takes place at a different instant. The closest encounter corresponds to some «encounter phase» $x_c \approx 0.60$. Due to approximate symmetry of the encountering the value $F_J(x_c) \approx 0$. Saturn's encounter phase is $y_c \approx 0.35$.

Effects of the two encounters can be separated off using the osculating values of comet's energy near perihelion which are also presented in Ref. [7]. The result is shown in Fig. 4 without the

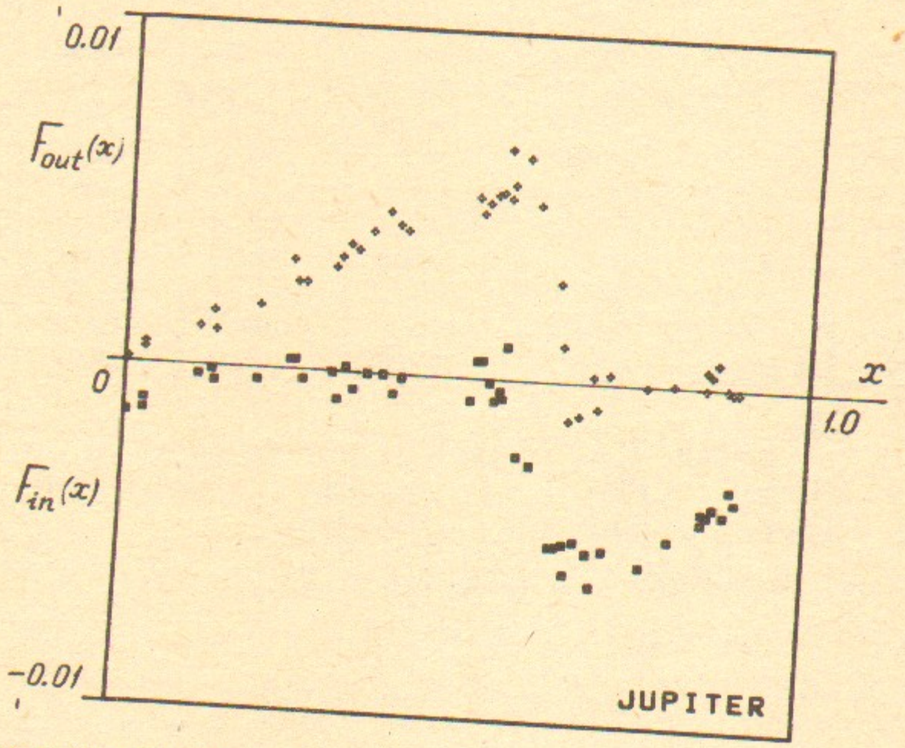

Fig. 4. The full perturbation of comet Halley, approaching the Sun (squares, $F_{in}(x)$), and moving away (diamonds, $F_{out}(x)$): $F_{in}+F_{out}=F(x)$ (Fig. 1).

separation of Saturn's perturbation. The particular shape of dependences in Fig. 4 is not completely clear to us.

Assuming the straight and uniform motion of both Jupiter and the comet at the right angle to each other for a very close encounter ($\sin i \ll 1$; $d_J \ll 1$) the following simple analytical relation for the perturbation

$$-F_J(x) = \frac{2A_J(x-x_c)\,d_J}{(x-x_c)^2+d_J^2}; \qquad F_J(x_c)=0;$$

$$A_J = \frac{4\sqrt{2}}{3}\,\frac{\mu_J}{\sin i} \approx 0.0060; \tag{7}$$

$$d_J = \sqrt{\frac{3}{2}}\,\frac{\sin i}{2\pi} \approx 0.059$$

can be shown to hold within some interval around x_c, including both $|F_J|$ maxima. Numerical values are given for the comet Halley. They agree quite well with Eqs (6), and do so still better with a more accurate FA presented in Fig. 2,*a* which gives $A_J \approx 0.0059$ and $d_J \approx 0.062$. Notice, however, that empirical function $F_J(x)$ is slightly asymmetric with respect to phase $x_c \approx 0.60$.

For Saturn's perturbation only the values of phase y_c, and of amplitude A_S in Eq. (7) change, namely

$$\frac{A_S}{A_J} = \frac{\mu_S}{\mu_J\, a_S} = 0.163, \tag{8}$$

where μ_S, a_S are the mass and orbit's radius for Saturn. The data in Fig. 2 give $A_S/A_J \approx 0.175$.

Even though Earth's mass $\mu_E \approx \mu_J/300$ is quite small, the close encounters with the comet do happen down to the minimal one, $\Delta_m \approx 0.04\,\mathrm{AU} \approx 0.008$ (in 837). In the latter case

$$\left(\frac{A_E}{A_J}\right)_{\max} \approx \frac{1}{2}\,\frac{\mu_E \sin i}{\mu_J \Delta_m} \approx 0.06, \tag{9}$$

which is 2 times the residual perturbation (5). However, the rms perturbation by Earth

$$\left(\frac{\langle F_E^2\rangle}{\langle F_J^2\rangle}\right)^{1/2} \approx \frac{1}{2}\,\frac{\mu_E}{\mu_J} \sin i\, \langle (1/\Delta)^2\rangle^{1/2} \approx 0.02 \tag{10}$$

is somewhat less than F_R. The value $\langle (1/\Delta)^2\rangle^{1/2} \approx 7.3\,(\mathrm{AU})^{-1} \approx 38$ is derived from the observational data cited in Ref. [9].

Some other planets (Venus, Uranus, Neptune) as well as the nongravitational forces (see Refs [7, 12]) provide a comparable perturbation. Altogether (Earth included) it amount to about $(\langle F_\Sigma^2\rangle / \langle F_J^2\rangle)^{1/2} \approx 0.025$ which is close to residual perturbation F_R of our model (see Eq. (5)). The latter includes, of course, the effect of

some other model approximations, particularly, the assumed circular rotation of Jupiter and Saturn.

At small w the perturbation $F(x)$ is nearly independent of w (7) as the energy exchange with Jupiter is determined by the «local» (osculating) speed of the comet $v^2 \approx 2 \gg w$. This was just the reason to choose quantity w as a dynamical variable of our model. Moreover, one can show that w is the so called ergodic variable (see Ref. [15], Section 13), and therefore the average perturbation $\langle F(x) \rangle \equiv 0$ was set zero (Table 2).

Notice that in presence of Saturn's perturbation one should either use the global phase X_n ($Y_n = r_S X_n$) in map (3), as we did, or add the equation $y_{n+1} = y_n + r_S w_{n+1}^{-3/2}$.

3. LOCAL INSTABILITY OF MOTION

Strong local instability of motion — the exponential divergence of close trajectories — is commonly accepted by now as the simplest and most reliable criterion of dynamical chaos, at least, in numerical experiments [1, 2, 5]. We studied this instability via the linearized equations of model (3):

$$\delta w_{n+1} = \delta w_n + F'(x_n^0) \cdot \delta x_n ,$$

$$\delta x_{n+1} = \delta x_n - \frac{3}{2} (w_{n+1}^0)^{-5/2} \cdot \delta w_{n+1} , \qquad (11)$$

where (x_n^0, w_n^0) is a reference trajectory, and $(\delta x_n, \delta w_n)$ the tangent vector $\vec{l}$. The nature of $\vec{l}$ dynamics is determined by the Lyapunov exponent

$$\Lambda = \lim_{n \to \infty} \frac{1}{n} \ln \frac{l_n}{l_0} . \qquad (12)$$

For a 2-dim. map $\Lambda = h$, the Kolmogorov—Sinai entropy. Dynamical chaos occurs under condition $h > 0$, or $\Lambda > 0$.

The motion under consideration has two very different time scales: i) $N_x \sim h^{-1}$ of the fast phase mixing, and ii) $N_w \gg N_x$ of a slow diffusion in w (Sect. 5). Therefore, the limit in Eq. (12) should be understood as a double strong inequality: $N_x \ll n \ll N_w$, while entropy $h(w)$ depends on comet's energy.

The eigenvalues of matrix (11) satisfy the condition $\lambda_1 \lambda_2 = 1$.

Define the largest eigenvalue modulus by λ_n; it depends on the iteration serial number n. Then:

$$\ln \lambda_n = |\ln |1 - k_n + \sqrt{k_n^2 - 2k_n}|| ;$$

$$k_n = \frac{3}{4} w_{n+1}^{-5/2} F'(x_n) , \qquad (13)$$

where we drop the superscript zero for the reference trajectory.

Consider first the perturbation by Jupiter only. In the STA (6)

$$k_n = \begin{cases} -\dfrac{0.108}{w_n^{5/2}} ; & 0.552 < x_n < 0.640 \\ \dfrac{0.0104}{w_n^{5/2}} ; & \text{otherwise} \end{cases} \qquad (14)$$

At the present value $w_n = w_1 \approx 0.3$ the instability occurs only within the phase interval given in the first line of Eq. (14) around encounter phase $x_c \approx 0.60$ where $\lambda_n \approx 6.2$. We shall term these phases unstable. For other x values $\lambda_n = 1$. Notice that with $k_n > 0$ for unstable phases the eigenvalue $\lambda_n \approx 1.9$ would be much smaller.

Using Eqs (13) and (14) we conclude that for

$$w_n < w_{cr} \approx 0.12 \qquad (15)$$

all the phases become unstable as $|k_n| > 2$. In this w domain there is a single solid chaotic component of motion.

On the contrary, at $w > w_{cr}$ large regions of stable motion arise around the fixed points of map (3): $w = w_m \approx m^{-2/3}$; $x = x_f$; $F_J(x_f) = 0$; $F_J'(x_f) > 0$ with m any integer (Fig. 5,*a*). The oscillation period about a fixed point $P_m \approx 2\pi m^{1/6} [(1 - 2d_J)/3A_J]^{1/2} \approx 700$ yr (in STA). Remnants of this periodicity persist in the chaotic component. Apparently, they were noticed and discussed in Refs [7, 16]. There are fixed points at phase x_c (7) as well, yet all the latter are unstable since $F_J'(x_c) < 0$.

In region $w > w_{cr}$ the motion instability grows only within the narrow interval of unstable phases (14), and the entropy can be described by the relation

$$h(w) \approx p(w) \ln [\alpha \lambda(w)] . \qquad (16)$$

Here $p(w)$ is the probability for a trajectory to enter the unstable phase interval; λ is the maximal eigenvalue in this interval which

does not depend on the phase in the STA (13); a factor $\alpha \sim 1$ depends only weakly on w, it describes the average orientation of $\bar{l}$ with respect to eigenvectors.

Numerical simulation at $w \approx 0.3$ gives: $h \approx 0.26$; $p \approx 0.19$; $\alpha \approx 0.55$ and $\lambda \approx 6.2$. Notice that probability p considerably exceeds the interval width $2d_J = 0.088$ (6). It is explained by a decrease in the area of chaotic component outside the unstable phase interval due to large stable regions there (Fig. 5,*a*). The α value is close to 1/2 which would correspond to the isotropic distribution of tangent

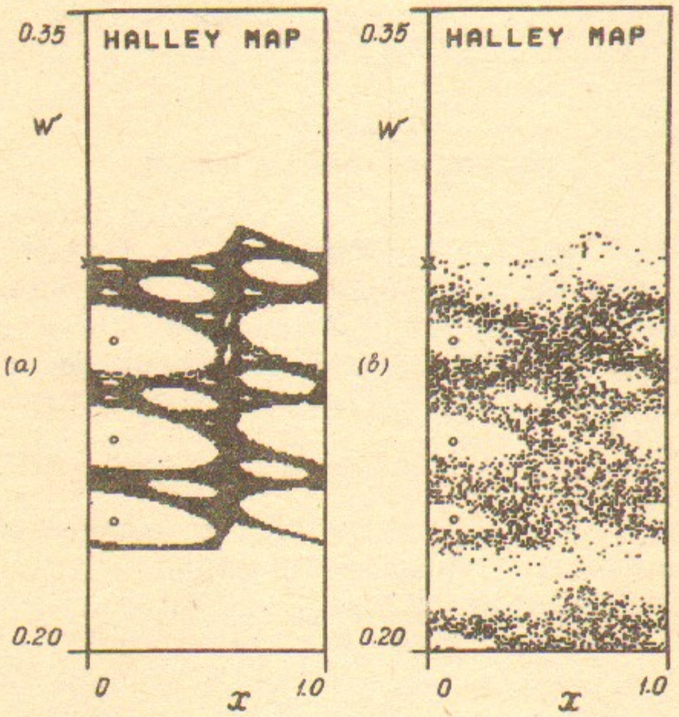

Fig. 5. Phase trajectory of map (3) in the STA (6). Initial conditions (crosses) $w_1 = 0.29164$; $x_1 = 0$ (in 1986, see Table 1): *a*) — Jupiter's perturbation only, $N = 1.5 \times 10^5$ iterations; *b*) — perturbation by both Jupiter and Saturn, $N = 4000$.

vector upon trajectory entering the unstable phase interval and assuming the eigenvectors to be orthogonal.

Comet's motion changes substantially if Saturn's perturbation is «switched on» (Fig. 5,*b*). Notice that upon including Saturn's perturbation the phase plane point (w, x) does no longer completely determine the trajectory which also depends on Saturn's phase y. In other words, the plane in Fig. 5,*b* is 2-dim. projection of the 3-dim. phase space of map (3) (see the end of Sect. 2). With Saturn's perturbation on, the stability domains noticeably decrease but persist. This leads to a reduction of the probability to $p \approx 0.13$ and, consequently, of the entropy to $h \approx 0.16$ while factor $\alpha \approx 0.53$ as well as the unstable eigenvalue λ remain nearly constant. The latter is explained by a weak Saturn's influence upon parameter k in Eq. (13):

$$\frac{\Delta k}{k} = \frac{A_S}{A_J} \frac{d_J}{d_S} r_S \approx 0.076. \qquad (17)$$

On the contrary, the perturbation by Earth, being relatively weak (9, 10) completely dominates nevertheless, upon a close encounter Δ with the comet as it is concentrated within a very narrow interval of phase $z = r_E X \bmod 1$ ($d_E \sim \Delta_m / 2\pi a_E \sim 0.006$). We have:

$$\left| \frac{k_E}{k_J} \right| \approx \frac{\mu_E}{\mu_J} r_E a_E \left(\frac{\sin i}{\Delta} \right)^2 \approx \frac{6.5 \times 10^{-4}}{\Delta^2} \lesssim 10,$$

$$\lambda \approx \lambda_E \approx 2 |k_E| \approx \frac{2.8 \times 10^{-3}}{\Delta^2} \lesssim 45. \qquad (18)$$

The latter numerical values correspond to minimal $\Delta = \Delta_m \approx 0.008 \approx 0.04$ AU. The approximation $\lambda_E \approx 2k_E$ holds for $\lambda_E \gg 1$.

Destabilizing effect of close encounters with Earth is well known from the practice of numerical simulation of comet's trajectory [7, 10, 12]. However, Earth's mean contribution to the entropy is insignificant. It can be roughly evaluated as follows. The observational data [9] reveal approximately homogeneous distribution of the encounters in Δ with the density $\varrho \approx 7$. Averaging over Δ we find

$$h_E \approx \varrho \int_{\Delta_m}^{\Delta_1} \ln [\alpha \lambda_E (\Delta)] \, d\Delta = 2\varrho (\Delta_1 - \Delta_m) - \varrho \Delta_m \ln [\alpha \lambda_E (\Delta_m)] \approx 0.06. \qquad (19)$$

Here $\alpha \approx 0.5$ (see Eq. (16)); $\lambda_E (\Delta_1) \approx 1/\alpha \approx 2$, whence $\Delta_1 \approx 0.025 \approx \approx 0.13$ AU from $k_E (\Delta_1) \approx +2.3$ (see Eq. (13)).

Within stability domains the motion is quasiperiodic, i. e. of a discrete spectrum, and w variation is strictly bounded and small while entropy $h = 0$. Interestingly, the present value of comet Halley's energy is only 3% above the nearest stability region. However, the residual perturbation F_R makes the existence of such regions questionable.

4. THE ERROR FACTOR IN NUMERICAL SIMULATION OF A CHAOTIC TRAJECTORY

The local instability of comet Halley's motion is the cause of its chaotic behaviour, particularly, of the diffusion in energy (Sections 5, 6). Moreover, the instability sharply restricts any extrapolation of comet's trajectory both forward and backward in time. The most error-sensitive quantity is perihelion passage time t_n, or the perturbation phase x_n. Just those t_n errors are given usually in the papers on numerical simulation of comet's dynamics [7, 8, 10, 12]. On the other hand, x_n errors significantly change the comet motion as the trajectory may get over from stable to unstable phases and vice versa. Define the error factor

$$f_m = \left| \frac{\delta x_m}{\delta x_0} \right| , \tag{20}$$

which describes the growth of phase errors over m comet's revolutions.

For $m \gg 1$ the mean error factor relates to the entropy (Sect. 3):

$$\bar{f}_m \approx e^{hm} . \tag{21}$$

Assume the maximal tolerable error $|\delta x_m|$ to be of the order of $d_J \approx 0.05$, $|\delta t_m| \sim 200$ days (a half-width of the unstable phase interval, see Eq. (6)). Then, the available length of extrapolation is restricted to

$$N_{ext} \approx \frac{1}{h} \ln \frac{d_J}{|\delta x_0|} \approx -6.3 \ln |\delta x_0| - 19. \tag{22}$$

It grows only logarithmically with the modelling accuracy $|\delta x_0|$. In Eq. (22) we use the value $h = 0.16$ without Earth's contribution (Sect. 3). Assuming an effective initial error $|\delta x_0| \approx 5 \times 10^{-4}$, $|\delta t_0| \approx 2$ days (see below) we obtain $N_{ext} \approx 29$ revolutions.

This estimate is rather crude, of course, due to big fluctuations on a relatively short time span, particularly, because of a narrow interval of unstable phases. A more accurate evaluation of the error factor can be performed as follows.

Consider linearized map (11) on some interval (t_n, t_m) using the «true» orbit (Table 1) as reference trajectory. Then, the error factor can be estimated, within this interval, as the biggest eigenvalue

modulus of the corresponding transfer matrix

$$f_{n,m} \sim \lambda_{n,m} . \tag{23}$$

The quantity $(\ln \lambda_{n,m})/(m-n) = h_{n,m}$ describes a «current» entropy on this interval (t_n, t_m). For instance, $h_{4,46} = 0.24$, which noticeably exceeds the mean value $h = 0.16$. The latter is reached in a longer time interval. The former value may be compared to $h = 0.30$ as measured by means of maps (3) and (11) (Sect. 3) for 50 comet's revolutions.

As the errors of linearized map also grow exponentially the transfer matrix is expedient to evaluate by multiplying the matrices of each iteration rather than numerically iterating map (11).

As a particular example we estimate the extrapolation accuracy for comet Halley's trajectory in Ref. [7]. The main parameters of this trajectory were determined from comet's apparitions in 1759, 1682 and 1607. However, the most error-sensitive quantity t_n was set to the observational value in 837 ($n = 16$). So, we assumed just the latter date as the extrapolation start in evaluating $\lambda_{16,m}$. These values are depicted in Fig. 6 for $m = 17-46$ (crosses) which correspond to the extrapolation back to -1403 in Ref. [7]. A peculiar feature of this dependence is rather long interval of stable motion ($\lambda = 1$, $m = 17-29$ except $\lambda_{16,25} = 1.89$) followed by a fairly steep instability. It is important to note that the earliest reliable observations of comet Halley fall just on the stable section (in -86, $m = 28$). In other words, the proper extrapolation, in absence of any observational data, gets actually into the unstable part of the trajectory. At the end of extrapolation the error factor amounts to $f_{16,44} \sim \lambda_{16,44} \approx 700$.

As the initial error δt_{in} it is natural to assume the rms deviation of computed t_m from their observational values within the stable interval $m = 17-28$. Using the data of Table 5 in Ref. [7] we find $\delta t_{in} = 2.7$ days. The values of $\ln(|\delta t_m|/\delta t_{in})$ are shown in Fig. 6 by squares.

At the end of extrapolation interval the error $|\delta t_{44}| \approx \approx \delta t_{in} \cdot f_{16,44} \sim 5$ yr becomes prohibitively large. The extrapolation holds, therefore, only up to about $m = 35$ (in -615) when $|\delta t_{35}| \sim 200$ days.

As a check of these estimates we made a similar extrapolation with our model (3). We have slightly corrected the value w_{16} in order to decrease δt_{25} (in 141) as well as it has been done in Ref. [7]. Actually, the eccentricity was corrected there but, curiously, both relative changes proved to be very close:

$|\Delta\varepsilon|/(1-\varepsilon)\approx|\Delta w|/w\approx 2.2\times10^{-4}$. The initial error for our model, calculated in the same way as above, $\delta t_{in}\approx 19$ days is in a reasonable agreement with the rms accuracy (5), and is only 7 times the error in Ref. [7]. A somewhat big error in the latter case is likely due to comet's encounters with Earth which are not included in our

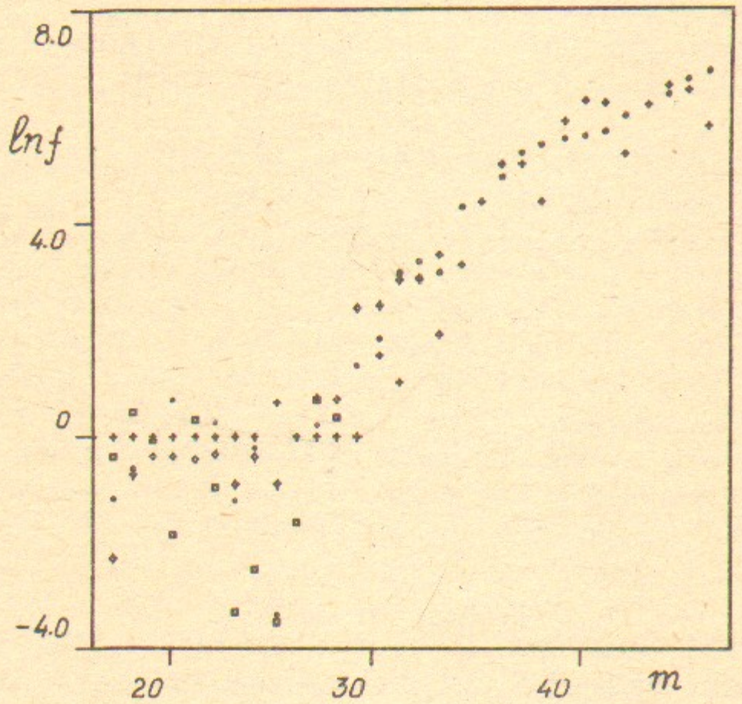

Fig. 6. Error factor f in extrapolation of comet Halley's chaotic trajectory (in 837 through −1403). Dependence of $\ln(|\delta t_m|/\delta t_{in})=\ln f$ vs. $m=17-46$ is shown after Refs [7] (squares); [12] (diamonds); our model (3) (full circles), and $\ln\lambda_{16,m}$ (crosses), see text.

model. The model values of $\ln(|\delta t_m|/\delta t_{in})$ are represented in Fig. 6 by full circles, and they clearly demonstrate a «sudden» burst of instability.

Finally, one may compare comet's trajectory in Ref. [7] with the recent computation in Ref. [12] (Table 8, sample I, for instance). The result is shown in Fig. 6 by diamonds. The rms difference between the two trajectories within the stable section is $\delta t_{in}=0.9$ day. At the end of extrapolation of the trajectory in Ref. [12] the error factor reaches the value $f_{16,33}\sim\lambda_{16,33}\approx 30$, and the separation of the trajectories becomes $|\delta t_{33}|\sim 27$ days. Why in the final version of comet's trajectory as presented in Table 9 of Ref. [12] the same separation lies within about one day remains a mystery for us.

In any event, all the above data definitely point out a rapid growth of the extrapolation errors in the time interval under consideration. This may explain some difficulties in reconciling the observational data in −465 and −617 with extrapolated trajectories of comet Halley as mentioned in Ref. [12].

We emphasize that the error growth in our model relates to the perturbation by Jupiter (and Saturn) only without any Earth's contribution which would increase the errors still more. We mention that the motion instability and error growth in a simple three-body model were noticed in Ref. [16] and certainly follow from the results of Ref. [6].

For comparison we note that the computational accuracy for the stable (quasiperiodic) motion of planets in the solar system on the same time interval is equivalent to $\delta t\sim 1$ day, and it weakly depends on time (see, e. g. Table 2 in Ref. [7]).

Contrary to extrapolation the interpolation of a chaotic trajectory can be realized to a much higher accuracy. Particularly, it is demonstrated by surprisingly small errors of our fairly simple model (3). How strange it may seem at the first glance, the interpolation is the simpler (requires the less changes in initial conditions and/or system's parameters) the stronger local instability of motion. It is the property of structural stability (robustness) of chaotic dynamics which also provides stability of the statistical description.

Notice that big absolute errors of t_n for the computed comet's trajectory in Ref. [7] do not prevent at all from using this trajectory for the reconstruction of perturbation $F(x)$ in Sect. 2. The point is that we need three successive values t_n only, and the reconstruction accuracy depends on trajectory errors within two comet's revolutions.

5. THE LOCAL DIFFUSION RATE OF A CHAOTIC TRAJECTORY

Within a chaotic component of comet's motion the perturbation (x) causes a diffusion in w. If perturbation phases x_n would be ot only random (which they are due to the local instability) but so statistically independent (which they generally are not in spite randomness) then the diffusion rate were determined simply by ean square of the perturbation (see, e. g., Refs [1, 2]):

$$D \equiv \frac{\langle (\Delta w)^2 \rangle}{m} = D_0 = \langle F^2(x) \rangle \approx \frac{A_J^2}{3} \approx 1.3 \times 10^{-5}. \qquad (24)$$

That limiting case holds at $w \ll w_{cr}$, when all the phases are unstable (Sect. 3). Here Saturn's contribution is negligibly small ($A_S^2/A_J^2 \approx 0.03$).

As w grows the entropy falls down (13) which results in a time correlation, and in diffusion deceleration. This becomes especially significant for $w > w_{cr}$ due to formation of domains with a regular motion (Fig. 5). It is just the case for the present value $w_1 \approx 0.3$.

We numerically measured the local (a small change in w) diffusion rate by averaging over 1024 trajectories of 46 iterations each with slighly different initial conditions. In the FA the rate $D(w_1) \approx 5.6 \times 10^{-6}$ while the STA gives 6.0×10^{-6}. It is about two times less than D_0 (24). «Switching-off» Saturn's perturbation somewhat decreases the diffusion (4.4×10^{-6}) due to a stronger correlation.

Residual perturbation F_R (Sect. 2) in the form of a random noise with the same rms magnitude doesn't change the rate: 5.5×10^{-6} (FA).

Finally, we directly used the data in Ref. [7] (Table 1) which is equivalent to one trajectory in the previous method. It gives a close value of 7.4×10^{-6}.

We also mention that at bigger w the diffusion rate drops, e. g., $D(0.7) \approx 2.7 \times 10^{-6}$.

6. GLOBAL DYNAMICS OF COMET HALLEY

Simple model (3) does not take any account of other orbit's parameters, besides w, and therefore its straightforward application is restricted by a relatively short time interval.

The most significant effect seems to be a periodic crossing of Jupiter's and comet's orbits due to the perihelion precession with a period $N_p \approx 440$ comet's revolutions (see Ref. [7]). This leads to a considerable decrease of the minimal Jupiter—comet distance s as compared to the present value $s_1 = \sin i \approx 0.3$.

Besides increase of the mean diffusion rate the prompt ejection of the comet out of the solar system may happen as a result of a single very close encounter with Jupiter. A rough estimate for the ejection probability can be derived as follows.

Consider analytical approximation (7) of perturbation with the parameters

$$A = \frac{A_1}{2}\frac{s_1}{s} = \frac{A_1}{2}\frac{d_1}{d}; \qquad d = d_1 \sin\left(\frac{2\pi m}{N_p}\right), \qquad (25)$$

where the present values are marked by subscript 1; m is the serial number of comet's revolution counting approximately from an orbits's crossing ($m_1 \approx N_p/4$), and factor 1/2 takes account of the fact that only one of the two encounters per turn can be close for $s \ll s_1$. The condition for ejection has the form $F < -w$, which is only possible at $|m| \lesssim A_1 N_p / 4\pi w \approx 0.7$ ($w = 0.3$) that is during about $8|m| \approx 6$ comet's revolutions per period $N_p = 440$. The ejection probability at such a special revolution is $p_1 \approx A_1 d_1 / w \approx 10^{-3}$ ($w = 0.3$). It is determined by entering a very narrow phase interval where $F < -w$. The ejection mean life time of the comet

$$N_{ej} \approx \frac{N_p}{8|m|p_1} \approx \frac{\pi}{2d_1}\left(\frac{w}{A_1}\right)^2 \approx 10^5 \qquad (26)$$

turns out to be surprisingly long, much in excess of the diffusion life time (see below). We mention that the probability for the comet to fall down on Jupiter is still about 100 times less.

To evaluate the mean diffusion rate in the independent-phase approximation we average expression (24) over m. Using Eq. (25) we obtain

$$\overline{D_0} \approx D_0 \cdot 6 d_1 \cdot \ln N_p \approx 2 D_0. \qquad (27)$$

Thus, the diffusion rate remains of same order in spite of orbits' crossing.

Using Eq. (13) for parameter k and perturbation approximation (7) and (25) it is easily verified that the width of the unstable phase interval does not depend on d. Therefore, the phase correlation persists for $d \ll d_1$ as well, and hence the actual mean diffusion rate $\overline{D}(w)$ is also of the order of $D(w)$ in the model (3).

Another omitted effect, which is important for the global dynamics, is apparently the diffusion in inclination i, as perturbation $F(x) \propto (\sin i)^{-1}$ (7). A rough estimate can be obtained from the data in Ref. [7] (Table 4). The maximal relative change over the time interval given is

$$\frac{\sin i_{max}}{\sin i_{min}} - 1 = 0.086$$

which is comparable with the corresponding diffusion change in w:

$$\frac{w_{max}}{w_{min}} - 1 = 0.111 .$$

Thus, even though the diffusion in i can hardly be neglected completely, it doesn't seem to change the order of magnitude for comet's life time in the solar system, especially in view of big fluctuations of the latter (see below).

In any event, we are going to make use of model (3) for some rough preliminary estimates of comet's global dynamics.

In the STA a connected chaotic component is unbounded in w because of a slow decay of perturbation Fourier harmonics [5, 13, 14]. For the true smooth perturbation the chaotic component is limited from above: $w \leqslant w_b$. Yet, the border is much higher than $w_1 \approx 0.3$, and therefore is unimportant here. Numerical simulation shows that, at any rate, $w_b > 0.6$ ($P_b < 2.15 = 25.5$ yr). What is important, that chaotic component extends down to $w = 0$, i. e. the comet leaves eventually the solar system along a hyperbolic orbit.

In the independent-phase approximation (24) the diffusion life time of the comet is

$$N_D \sim \frac{w^2}{D_0} \approx \frac{3w^2}{A_J^2} \lesssim 10^3 ,$$

$$t_D = N_D \langle w^{-3/2} \rangle \approx \frac{4N_D}{w^{3/2}} \sim 3 \times 10^5 \sqrt{w} \lesssim 10^6 \text{ yr} \qquad (28)$$

where the initial $w \lesssim w_{cr} \approx 0.12$ ($P_{cr} \approx 290$ yr).

It is interesting to compare N_D with the ejection time (26):

$$\frac{N_D}{N_{ej}} \approx 2d_1 \approx 0.1 . \qquad (29)$$

Notice, that even though Eq. (26) for N_{ej} has a «diffusion appearance» it is not necessarily related to any chaotic motion, and it holds for regular trajectories as well provided the phase x runs over the whole interval, i. e. is rotating.

The diffusion proceeds down to $w_{min} \sim A_J \approx 0.006$ which corresponds to comet's period $P_{max} \sim 2.6 \times 10^4$ yr, and to its aphelion $2a_{max} \sim 1700$ AU.

We carried out numerical simulation of the global dynamics using 40 trajectories of map (3) with initial conditions from Table 1. Because of the local instability all these trajectories rapidly diverge and show quite different values of the life time:

$$1374 \leqslant N_D < 10^5 , \quad 5.3 \times 10^5 \lesssim t_D \text{ (yr)} < 2 \times 10^7 .$$

The latter relates to big diffusion fluctuations, especially, at $w > w_{cr}$. An example of the full phase trajectory, projected onto plane (w, x), is depicted in Fig. 7,*a*.

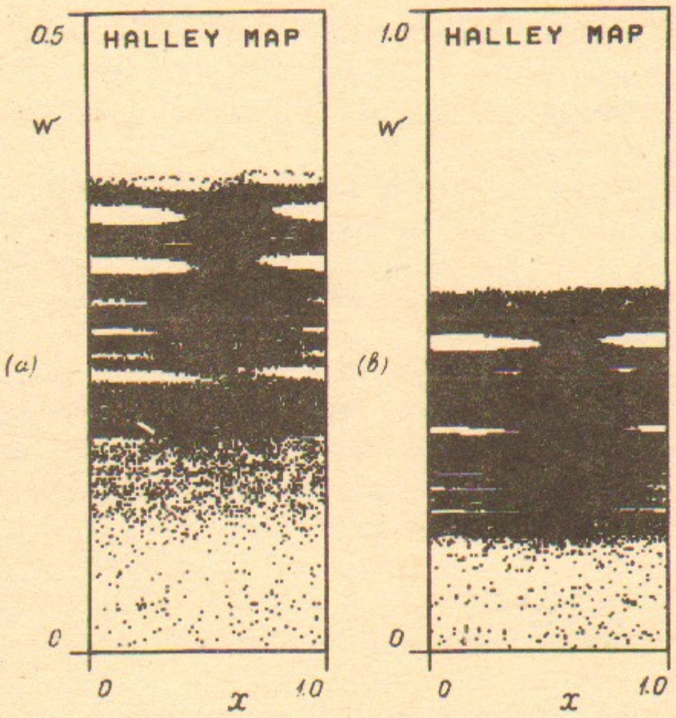

Fig. 7. Two examples of comet Halley's global dynamics in model (3), $N_D \approx 4.1 \times 10^4$, $t_D \approx 4.5 \times 10^6$ yr (*a*); with a variable nongravitational acceleration (30), $\overline{F} = 3 \times 10^{-5}$, $N_{ev} = 10^3$, $\tilde{N}_{Dd} \approx 3.1 \times 10^5$, $\tilde{t}_{Dd} \approx 2.1 \times 10^7$ yr (*b*).

The mean diffusion life time of the comet is equal to

$$\overline{N_D} \approx 1.8 \times 10^4 ; \quad \overline{t_D} \approx 3.9 \times 10^6 \text{ yr}$$

the average period being $\overline{P_D} \approx \overline{t_D} / \overline{N_D} \approx 220$ yr, and the mean rate of global diffusion $\overline{D_G} \approx w_1^2 / \overline{N_D} \approx 5 \times 10^{-6}$. The latter is close to the local diffusion rate (Sect. 5).

The global diffusion primarily proceeds downwards in w because of increasing of $D(w)$ in this direction.

Comet's life time, unlike the local diffusion rate, crucially depends on a relatively weak perturbation by Saturn. Upon its «switching-off» the life time jumps up to $\overline{N_D} \approx 6 \times 10^5$ ($\overline{t_D} \approx 6 \times 10^7$ yr), i. e. by a factor of 20, due to a long-time «sticking» of trajectory in some narrow w layers. Under these circumstances even a weak additional perturbation may greatly change the life time. Notice that comet's mean period $\overline{P_D} \approx 100$ yr remains close to the initial $P_1 \approx 76$ yr.

As the diffusion proceeds symmetrically in the both directions of time, the full sojourn time of the comet in the solar system is twice as big, $2\overline{N_D}$, which, of course, is of the same order on the background of big fluctuations.

Certainly, comet's actual life time may be determined by totally different physical processes, for example, simply by its evaporation. After recent data in Ref. [17] the evaporation time amounts to $N_{ev} \approx 4000$ comet's revolutions only. However, there is no such a limitation backwards in time.

Another important effect is a systematic variation of w (a drift). The physical cause of the drift is the so called transverse nongravitational acceleration (force) related to evaporation of the comet near the Sun [18]. Using the latest data on the parameters of nongravitational forces [8, 12] we find

$$\overline{\frac{dw}{dn}} = \overline{F(x)} \approx +3 \times 10^{-5}$$

backward in time. Forward in time $\overline{F} < 0$ which would result in comet's leaving the solar system after about $N_d \approx w_1 / \overline{F} \approx 10^4$ revolutions, that is somewhat less than $\overline{N_D} \approx 1.8 \times 10^4$. The combination of both diffusion and drift would decrease the life time still more; numerically, $\overline{N_{Dd}} \approx 6600$.

We mention that the change in phase volume (dissipativity), which is inevitably related to the drift, is, nevertheless, much smaller, so that the corresponding time N_{dis} can be shown to have the order $N_{dis}/N_d \sim (qw)^{-1} \sim 30$ where $q \approx 0.6$ AU ≈ 0.12 is comet's perihelion distance. Hence, map (3) can be treated as canonical one even in presence of the drift.

The effect of drift is much stronger backward in time ($\overline{F} > 0$). In this case, w variation is eventually determined by the drift only, that is w continuously grows after some time because of a sharp decrease in the diffusion rate with w (Sect. 5).

Now, we take into account a possible time-variation of the nongravitational forces. It may occur due, for example, to decreasing of comet's mass because of evaporation which could result in increasing of the nongravitational acceleration. A natural time scale for that process would be the evaporation time $N_{ev} \approx 4000$ comet's revolutions [17]. On this ground we modified the drift equation as follows (backward motion, $\overline{F} > 0$):

$$\overline{\frac{dw}{dn}} = \frac{\overline{F}}{1 + \frac{n}{N_{ev}}} = \tilde{F}(n) . \qquad (30)$$

Decreasing of the drift speed $\tilde{F}$ with n leads eventually to a purely diffusive motion. Yet, comet's life time considerably increases as compared to that without drift. This is because the drift, decreasing though, still has enough time to move the comet to a bigger w where the diffusion rate sharply drops.

According to numerical simulation, the life time for Eq. (30) is $\tilde{N}_{Dd} \gtrsim 5 \times 10^5$. Even upon reducing N_{ev} to 10^3 the mean life time $\tilde{N}_{Dd} \approx 1.4 \times 10^5$ is still much longer than $\overline{N_D} \approx 1.8 \times 10^4$. An example of the latter trajectory with $\tilde{N}_{Dd} = 3.1 \times 10^5$ is given in Fig. 7,*b*. Under these circumstances the variation of inclination i as well as the single ejection of the comet by Jupiter (26) play an important role. These questions require further more thorough studies.

7. CONCLUSION

A fairly simple model for comet Halley's dynamics, developed in the present paper, allows to study essential features of its short- and long-term evolution in both directions of time. Numerical simulation as well as the analytical calculations reveal that comet's motion is chaotic, and allow to evaluate the error growth in the extrapolation of its trajectory. We would like to emphasize again that the mean error growth is determined primarily by Jupiter's perturbation, and not by comet's encounters with Earth which seems to be

a common belief (see, e. g., Refs [7, 12]). Also, for any chaotic trajectory the mean error growth in time is exponential but not a power law one as is sometimes assumed [19]. Increasing the computation accuracy helps, therefore, only on a short time interval as is easily verified by a slight change in initial conditions or by the time reversal.

Since chaotic motion has a continuous temporal Fourier spectrum, the so called «cyclic method», i. e. the search of commensurabilities in motions of the comet, Jupiter and Saturn [20] is totally inaplicable here. This displays a qualitative distinction of chaotic motion from a regular (quasiperiodic) one, as the planet motion, for example, where this method is successfully used. We remind that the perturbation in our model is a regular (quasiperiodic) function of time except a small residual perturbation, assumed to be random, which however doesn't change the chaotic nature of comet's motion.

Dynamical chaos results in the diffusion of comet's orbit in both directions of time, so that the comet is found eventually outside the solar system. Numerical simulation shows that comet's sojourn time within the solar system crucially depends on a weak nongravitational force acting upon the comet near the Sun. Interestingly, repeated crossings of comet's and planet's orbits only insignificantly decrease the comet life time.

All the computations have been performed on a fast personal computer «Odroenok» designed and manufactured in the Institute of Nuclear Physics at Novosibirsk [21]. We are greatly indebted to A.N. Aleshaev, S.D. Belov, V.P. Kozak, E.A. Kuper, G.S. Piskunov, and S.V. Tararyshkin for numerous advices and continual assistance.

We also acknowledge interesting and helpful discussions with F.M. Izrailev and D.L. Shepelyansky.

REFERENCES

1. *Lichtenberg A.J. and Lieberman M.A.* Regular and Stochastic Motion.—N.Y.: Springer, 1983.
2. *Zaslavsky G.M.* Chaos in Dynamic Systems.—N.Y.: Harwood, 1985.
3. Physics Today 38 N 9 (1985) 17.
4. *Arnold V.I.* Dokl. Akad. Nauk SSSR 156 (1964) 9.
5. *Chirikov B.V.* Phys. Reports 52 (1979) 263.
6. *Petrosky T.Y.* Phys. Lett. A117 (1986) 328.
7. *Yeomans D.K., Kiang T.* Mon. Not. R. Astr. Soc. 197 (1981) 633.
8. *Kalyuka Yu.F., Tarasov V.P., Tikhonov V.F.* Astron. Zh. (Pisma) 11 (1985) 788.
9. *Belyaev N.A., Churyumov K.I.* Halley's Comet and its Observation.—Moskva: Nauka, 1985.

10. *Brady J.L. and Carpenter E.* Astron. J. 76 (1971) 728.
11. *Kiang T.* Mem. R. Astr. Soc. 76 (1971) 27.
12. *Landgraf W.* Astron. Astrophys. 163 (1986) 246.
13. *Chirikov B.V., Keil E. and Sessler A.M.* J. Stat. Phys. 3 (1971) 307.
14. *Chirikov B.V., Izrailev F.M.* In: Colloques Intern. du CNRS., N 229, (Toulouse, 1973). Paris, 1976, p.409.
15. *Chirikov B.V.* In: Topics in Plasma Theory, v.13; Ed. Kadomtsev B.B., Moskva: Energoatomizdat, 1984, p.3.
16. *Kiang T.* In: Dynamics of the Solar System.—IAU Symp., N 81, Dor t, Holland, 1979, p.303.
17. *Boyarchuk A.A., Grinin V.P., Zvereva A.M. et al.* Astron. Zh. (Pisma) 12 (1986) 696.
18. *Marsden B.G., Sekanina Z. and Yeomans D.K.* Astron. J., 78 (1973) 211.
19. *Kazimirchak-Polonskaya E.I.* In: Astrometry and Celestial Mechanics.—Moskva: Nauka, 1978, p.340.
20. *Kamieński M.* Acta Astron. 12 (1962) 227.
21. *Piskunov G.S., Tararyshkin S.V.* Avtometria, 1986, N 4, p.32.

B.V. Chirikov and V.V. Vecheslavov

Chaotic Dynamics of Comet Halley

В.В. Вечеславов и Б.В. Чириков

Хаотическая динамика кометы Галлея

Ответственный за выпуск С.Г.Попов

Работа поступила 23 декабря 1986 г.
Подписано в печать 30.12.1986 г. МН 11920
Формат бумаги 60×90 1/16 Объем 1,5 печ.л., 1,2 уч.-изд.л.
Тираж 290 экз. Бесплатно. Заказ № 6

Набрано в автоматизированной системе на базе фотонаборного автомата ФА1000 и ЭВМ «Электроника» и отпечатано на ротапринте Института ядерной физики СО АН СССР,
Новосибирск, 630090, пр. академика Лаврентьева, 11.